

Article

The Structure and Function of Biomaterial Endolysin EFm1 from *E. faecalis* Phage

Xuerong Zhou ¹, Xiaotao Zeng ², Li Wang ¹, Yanhui Zheng ², Guixiang Zhang ³ and Wei Cheng ^{1,2,*}

¹ State Key Laboratory of Biotherapy, Sichuan University, Chengdu 610041, China; xuerong_zhou@163.com (X.Z.); 900592@163.com (L.W.)

² Division of Respiratory and Critical Care Medicine, Respiratory Infection and Intervention Laboratory of Frontiers Science Center for Disease-Related Molecular Network, State Key Laboratory of Biotherapy, West China Hospital of Sichuan University, Chengdu 610041, China; zengxt@scu.edu.cn (X.Z.); yahuzheng@outlook.com (Y.Z.)

³ Laboratory of Bariatric and Metabolic Surgery, Department of Gastrointestinal Surgery, West China Hospital, Sichuan University, No. 37, Chengdu 610041, China; zhangguixiang@wchscu.cn

* Correspondence: chengwei669@scu.edu.cn; Tel.: +86-182-1566-0676

Citation: Zhou, X.; Zeng, X.; Wang, L.; Zheng, Y.; Zhang, G.; Cheng, W. The Structure and Function of Biomaterial Endolysin EFm1 from *E. faecalis* Phage.

Materials **2022**, *15*, 4879.

<https://doi.org/10.3390/ma15144879>

Academic Editors: Satoshi Komasa, Yoshiro Tahara, Tohru Sekino, Joji Okazaki, Francesco Baino

Received: 27 May 2022

Accepted: 8 July 2022

Published: 13 July 2022

Publisher's Note: MDPI stays neutral with regard to jurisdictional claims in published maps and institutional affiliations.



Copyright: © 2022 by the authors. Licensee MDPI, Basel, Switzerland. This article is an open access article distributed under the terms and conditions of the Creative Commons Attribution (CC BY) license (<http://creativecommons.org/licenses/by/4.0/>).

Abstract: The endolysin EFm1 from the *E. faecalis* 002 (002) phage IME-EF1 efficiently lyses *E. faecalis*, a gram-positive bacterium that severely threatens human health. Here, the structure and lytic activity of EFm1 toward *E. faecalis* were further investigated. Lytic activity shows that EFm1 specifically lyses 002 and 22 other clinically isolated *E. faecalis*, but not *E. faecalis* 945. Therefore, EFm1 may be an alternative biomaterial to prevent and treat diseases caused by *E. faecalis*. A structural analysis showed that EFm1_{D166Q} is a tetramer consisting of one full-length unit with additional C-terminal domains (CTDs), while EFm1_{166–237 aa} is an octamer in an asymmetric unit. Several crucial domains and novel residues affecting the lytic activity of EFm1 were identified, including calcium-binding sites (D20, D22 and D31), a putative classic amidohydrolase catalytic triad (C29, H90 and D108), a tetramerization site (M168 and M227), putative ion channel sites (IGGK, 186–198 aa), and other residues (R208 and Y209). Furthermore, EFm1 exhibited no significant activity when expressed alone in vivo, and IME-EF1 lytic activity decreased when *efm1* was knocked down. These findings provide valuable insights into the molecule mechanism of a potential functional biomaterial for the treatment of the disease caused by the opportunistic pathogen *E. faecalis*.

Keywords: *E. faecalis*; endolysin EFm1; crystal structure; lytic activity; CRISPR interference

1. Introduction

The emergence of antimicrobial resistance in microorganisms is a global concern and poses a serious threat to public health [1,2]. *E. faecalis*, a gram-positive bacterium that is commonly present in humans and animals, is an opportunistic pathogen that causes community and hospital-acquired infections and can be life-threatening to immunocompromised patients [3]. The cell wall of *E. faecalis* is mainly composed of peptidoglycan, teichoic acid and lipoteichoic acid. Lipoteichoic acid has a negative charge and is covalently bound to the cell membrane; its chain extends into the cell wall [4]. It is extremely difficult to use routine antibiotics to eliminate *E. faecalis* strains with high levels of antibiotic resistance, especially vancomycin-resistant *E. faecalis* (VREF) [5]. By modifying the binding site, D-alanyl-D-alanine (terminal residues of stems) was converted to D-alanyl-D-lactic acid in vancomycin-resistant *E. faecalis*, resulting in a 1000-fold decrease in its binding affinity for vancomycin [6]. Mobile genetic elements, including plasmids and transposons, play a critical role in the spread and persistence of drug resistance in *E. faecalis* [7]. Therefore, the search for new drugs to treat infections caused by this opportunistic pathogen is urgent.

Phage therapy is regarded as a feasible alternative treatment option when antibiotics are ineffective against bacterial infections, and endolysin (lysin) therapy is an important part of this strategy [8]. Phage-encoded endolysins are highly evolved peptidoglycan hydrolases that lyse the host cell at the terminal stage of the phage lytic lifecycle to ensure the release of phage progeny [9]. Endolysins are considered alternative therapeutic agents for use against organisms with drug tolerance [10]. Endolysins not only show high lytic potential against numerous bacterial species, but also provide an approach to eliminate biofilms [11]. There are several advantages associated with the use of endolysin to treat infections caused by this opportunistic pathogen, such as high efficiency and specificity, low resistance and few neutralizing antibodies [12]. Normally, lysin cannot remain in a stable state at room temperature. However, after bonding to a surface or inside specific materials, its stability is improved, making it a functional biomaterial [13].

An *E. faecalis* 002 (002) bacteriophage (phage) named IME-EF1 was isolated from hospital sewage. A whole-genome sequence analysis showed that this phage belonged to the *Siphoviridae* family; it was found to be highly homologous with *E. faecalis* phage SAP6 and *E. faecalis* phage BC-611 [14]. EFm1, a lysin of IME-EF1, is similar to the lysin from SAP6 and BC-611 in the predicted amino acid sequence and conserved domain [14]. These three lysins all have a conserved CHAP (cysteine-histidine-dependent amido-hydrolase/peptidase) domain in the N terminal, while EFm1 possesses a much broader bactericidal spectrum including two VREF strains (*E. faecalis* V583). Similar to LysEF-P10 [14], EFm1 decreased fatality rates to 20% within 30 min after intraperitoneal injections were given to mice with 002 [15]. Zhou et al. reported that EFm1 exhibited a unique architecture in which one full-length forms a tetramer with three additional C-terminal cell-wall binding domains (CBD). EFm1 contains an internal ribosomal binding site upstream of a putative alternative start codon, which is responsible for the additional CBDs that are important for its activity [16].

Therefore, EFm1 is expected to be a novel drug to treat diseases caused by the ectopic parasitism of *E. faecalis*, such as sepsis and urinary tract infections. However, the lytic spectrum of EFm1 to *E. faecalis*, the crucial domains and residues affecting its lytic activity and its role in phage IME-EF1 infection need to be further explored. In this study, the *E. faecalis* 945 strain resisted to EFm1 was obtained by a deep broadening of the cleavage spectrum of EFm1. Additionally, the lytic mechanism of EFm1 was identified by determining the structures of EFm1_{D166Q} and EFm1_{166–237aa}, analyzing their lytic activity and verifying the activity of *efm1* in 002 and IME-EF1.

2. Materials and Methods

2.1. Phage and Strains

The *E. faecalis* phage IME-EF1 (GenBank accession number: NC_041959.1) and cultures of the *E. faecalis* strains 002, 19, 255, 281, 284, 285, 410, 436, 462, 620, 630, 673, 697, 850, 863, 945, 1550, 1590, 1591, 1592, 1593 and 1763 were acquired from Tong Yi Gang (Anhui Medical University). The *E. faecalis* strains V583 and ATCC29212 were obtained from Huang Xiao Jing (Fujian Medical University) and Cheng Li (West China School/Hospital of Stomatology Sichuan University), respectively. *E. faecalis* cultures were inoculated at 37 °C in brain heart infusion (BHI) medium (USA, BD Difco; for 1 L total: 7.7 g of calf brain, infusion from 200 g; 9.89 g of beef heart, infusion from 250 g; 10.0 g of proteose peptone; 2 g of dextrose; 5.0 g of sodium chloride; and 2.5 g of disodium phosphate; final pH 7.4 ± 0.2). *E. coli* BL21(DE3) and *B. subtilis* CU1050 [17] were preserved in our laboratory and cultured in Luria-Bertani (LB) medium (for 1 L total: 10 g of NaCl (China, Dragon), 10 g of tryptone (USA, OXOID), 5 g of yeast extract (USA, OXOID)).

2.2. Plasmid Construction

The codon-optimized *efm1* (GenBank accession number: YP_009603970) from IME-EF was synthesized by GENEWIZ and cloned into the vector pGEX-6P-1 (addgene plasmid: 113500) to produce the plasmid pGEX-EFm1. All plasmids expressing EFm1 mutants were constructed by the Quik Change method with the corresponding primers using pGEX-EFm1 as a template [17]. The primers used in this study are listed in Table 1. The sequences of all constructs used in this study were confirmed by DNA sequencing. The operations performed were as follows:

Table 1. Primers used in this study.

Name	Sequence (5' to 3')	Usage
EFm1 _{1–165aa} -F	AGACGATTAGCTCGAGCGGCCGCATCGT	pGEX-EFm1 _{1–165 aa}
EFm1 _{1–165aa} -R	GCTCGAGCTAATCGTCTCCTTTAAATTGTCCTAGATT	
EFm1 _{165–237aa} -F	CTGGGATCCGATGATATTATGTTTCATCTATTACAAACGCAC	pGEX-EFm1 _{165–237 aa}
EFm1 _{165–237aa} -R	ATATCATCGGATCCCAAGGGCCCCCTG	
EFm1 _{Δ145–165aa} -F	GCGTTTGTAATAGATGAACATAATATCTGAAGCAGCTTCGTAAGG	pGEX-EFm1 _{Δ145–165aa}
EFm1 _{Δ145–165aa} -R	GATATTATGTTTCATCTATTACAAACGCACTAAGCAAGGA	
EFm1 _{D166Q} -F	GAGACGATCAAATTATGTTTCATCTATTACAAACGCACTAA	pGEX-EFm1 _{D166Q}
EFm1 _{D166Q} -R	CATAATTTGATCGTCTCCTTTAAATTGTCCTAGATT	
EFm1 _{C29A} -F	TACGCAAGCGATGGACTTGACAGTAGACGTTATGCA	pGEX-EFm1 _{C29A}
EFm1 _{C29A} -R	AGTCCATCGCTTGGTACCATAACCATCCGTC	
EFm1 _{H90A} -F	ATATGGTGCGACAGGTATCGCAACAGAGGATGG	pGEX-EFm1 _{H90A}
EFm1 _{H90A} -R	TACCTGTCGCACCATATTGAGCATAGTATCCTAAGCC	
EFm1 _{D108A} -F	CAGTGTTCGCAAAACATGGATTAAACCAAGCC	pGEX-EFm1 _{D108A}
EFm1 _{D108A} -R	AGTTTTGCGCAACACTGACAAAGGTTCCGTCAG	
EFm1 _{D20A} -F	AAAGGCGTGGCGGCTGACGGATGGTATGGTACG	pGEX-EFm1 _{D20A}
EFm1 _{D20A} -R	TCAGCCGCCACGCCTTTCCGACAAGG	
EFm1 _{D22A} -F	ACGCTGCGGGATGGTATGGTACGCAATGTATG	pGEX-EFm1 _{D22A}
EFm1 _{D22A} -R	ATACCATCCCGCAGCGTCCACGCCTTTTCC	
EFm1 _{W24A} -F	TGACGGAGCGTATGGTACGCAATGTATGGACTTGA	pGEX-EFm1 _{W24A}
EFm1 _{W24A} -R	TACCATACGCTCCGTCAGCGTCCACGCC	
EFm1 _{G26A} -F	TGACGGAGCGACGCAATGTATGGACTTGACAGTAG	pGEX-EFm1 _{G26A}
EFm1 _{G26A} -R	ATTGCGTCGCTCCGTCAGCGTCCACGCC	
EFm1 _{D31A} -F	GTACGCAATGTATGGCCTTGACAGT	pGEX-EFm1 _{D31A}
EFm1 _{D31A} -R	ACGCTACTGTCAAGGCCATACATT	
EFm1 _{M168A} -F	GAGACGATGATATTGCGTTCATCTATTACAAACGCACTAAGCA	pGEX-EFm1 _{M168A}
EFm1 _{M168A} -R	CGCAATATCATCGTCTCCTTTAAATTGTCC	
EFm1 _{M227A} -F	TTGAAGGCGATGGAAGCAGCTTTACCACAAGT	pGEX-EFm1 _{M227A}
EFm1 _{M227A} -R	GCTTCCATCGCCTTCAATCCAAAGTTGTCGTGGT	
EFm1 _{M227K} -F	GAAGAAGATGGAAGCAGCTTTACCACAAGT	pGEX-EFm1 _{M227K}
EFm1 _{M227K} -R	CTGCTTCCAICTCTTCAATCCAAAGTTGTCGTGGT	
EFm1 _{K173E} -F	CTATTACGCGCGCACTAAGCAAGGAAGCACT	pGEX-EFm1 _{K173E}
EFm1 _{K173E} -R	TAGTCCGCTCGTAATAGATGAACATAATATCATCGTCTCC	
EFm1 _{K176E} -F	ACGCACTGAGCAAGGAAGCACTGAGCAATGG	pGEX-EFm1 _{K176E}
EFm1 _{K176E} -R	TTCCTTGTVVAGTGGCTTTGTAATAGATGAACATAATATC	
EFm1 _{R190E} -F	GAGGTAAAGAGATCTACTTACCAACAATGACTTACGTAAAC	pGEX-EFm1 _{R190E}
EFm1 _{R190E} -R	GTAGATCTCTTTACCTCCAATAACGAACCATTG	
EFm1 _{K236E} -F	AGTTGAGGTATAGCTCGAGCGGCCGC	pGEX-EFm1 _{K236E}
EFm1 _{K236E} -R	CGAGCTATACCTCAACTGTGGTAAAGCTGCTTCCA	
EFm1 _{I186A-K189A} -F	ACTGAGCAATGGTTTCGTTCTGATCTACTTA	pGEX-EFm1 _{I186A-K189A}
EFm1 _{I186A-K189A} -R	TGTTGGTAAAGTAGATACGAACGAACCATTG	
EFm1 _{Y209A} -F	GACCTTATCAAACGAGCTGGTGGAA	pGEX-EFm1 _{Y209A}
EFm1 _{Y209A} -R	GTTAGTGTTCACCAAGCTCGTTG	
EFm1 _{R208A} -F	GCATATGGTGGAACACTAACGTAACGA	pGEX-EFm1 _{R208A}
EFm1 _{R208A} -R	GTGTTTCCACCATATGCTTTGATAAGGTCGTTAGCTTCGTT	
pDL278-EFm1-F	GAGCTCGGTACCCGGGGATCCCTATACTTTAACTTGTGGTAAA	pDL278-EFm1
pDL278-EFm1-R	ACCATGATTACGCCAAGCTTAATGGTTAAATTAACGATGTA	
dCas9-F	GACCATGATTACGCCAAGCTTAATGGACAAGAAGTACAGCATCGGC	pDL278-dCas9
dCas9-R	GAGCTCGGTACCCGGGGATCCCTAGTCGCCGCCAGCTG	

pDL278-F	ATGACCATGATTACGCCAAGCTTAATGGACAAGAA	Linearized pDL278-dCas9
pDL278-R	TTGTTATCCGCTCACAAATCCACACAACATACGAG	
sgRNA-F	GAATTGTGAGCGGATAACAAGACGTTATGCAACGCTTCTTGTGTTTAGAGCTAGAAATAGCAAG	pDL278-dCas9-sgRNA
sgRNA-R	CITGGCGTAATCATGGTCATCAAAAAAGCACCGACTCGG	

The XtalPred [18] and SERP [19] servers were used to predict disordered loops and identify high-entropy surface patches of EFm1, since the wild-type EFm1 crystal could not be harvested in our experiment. Based on the results, the D166Q mutant of EFm1 was used for crystallization; the plasmid pGEX-EFm1_{D166Q} was constructed using the primers EFm1_{D166Q}-F/R, and the purified protein was used to solve the crystal structure of EFm1_{D166Q}.

The *efm1* fragment was amplified with the primers pDL278-EFm1-F/R from the plasmid pGEF-6P-1 and cloned into the plasmid pDL278 (addgene plasmid: 46882) to produce pDL278-*efm1*. CRISPR interference (CRISPRi) was used to interfere with the expression of *efm1* in vivo with the plasmid pDL278-dCas9-sgRNA. The dCas9 fragment was amplified with the primers dCas9-F/R from the plasmid pRH2502 (addgene plasmid: 84379) and cloned into the plasmid pDL278 to produce pDL278-dCas9. Subsequently, the plasmid pDL278-dCas9 was linearized by amplification with the primers pDL278-F/R. The sgRNA scaffold containing *efm1*-targeting sgRNA was amplified with the primers sgRNA-F/R from the plasmid pJMP3-yorR [17], which was previously constructed by our laboratory and cloned into linearized pDL278-dCas9 to produce pDL278-dCas9-sgRNA.

2.3. Protein Expression and Purification

The expression and purification of EFm1 were performed as previously described with minor modifications [17,20]. The isoelectric point (pI) of EFm1 predicted by EditSep software was 6.75. A single colony of *E. coli* BL21 (DE3) containing a plasmid encoding wild-type EFm1 or a variant was inoculated into 10 mL of LB medium with 100 µg/mL ampicillin and grown for 12–15 h at 37 °C. Then, the culture was used to inoculate 1 L of LB medium with 100 µg/mL ampicillin. Cultures were grown at 37 °C until the absorbance at 600 nm (OD_{600 nm}) reached 0.6–0.8. Cultures were grown at 16 °C for 18 h, and isopropyl β-D-thiogalactoside (IPTG) was added at a final concentration of 3 mM to induce protein expression. Harvested cell pellets were resuspended and lysed by sonication in buffer A (25 mM Tris-HCl, 200 mM NaCl; pH 8.0). Then, the cell lysate containing the N-terminal GST-EFm1 protein was applied to glutathione-coated Sepharose resin (GE Healthcare) and washed in buffer A. Subsequently, the protein was assessed by anion exchange chromatography (Source Q; GE Healthcare) with buffer B (25 mM Tris-HCl; pH 8.0) and buffer C (25 mM Tris-HCl, 2 M NaCl; pH 8.0) and size-exclusion chromatography (columns from GE Healthcare) with buffer A for further purification. The peak fractions were collected and assessed by sodium dodecyl sulfate–polyacrylamide gel electrophoresis (SDS-PAGE). The clear fractions were pooled and flash frozen in liquid nitrogen for crystallization. Selenomethionine (Se-Met)-substituted proteins were expressed in M9 medium (5 × M9, for 1 L total: 44.3 g of Na₂HPO₄ (China, Dragon), 19.5 g of KH₂PO₄ (China, Dragon), 3.25 g of NaCl (China, Dragon), 6.5 g of NH₄Cl (China, Dragon)).

2.4. Crystallization and Structure Determination

Crystals of EFm1_{D166Q} (15 mg/mL) and the C-terminal domain EFm1_{166–237 aa} (10 mg/mL) were grown at 16 °C by the sitting drop method, with one precipitant consisting of 0.1 M HEPES (pH 7.0–7.2), 0.2 M NaCl and 18–22% poly (ethylene glycol) 6000 and another consisting of 20% PEG 3350 and 0.2 M KCl. The Se-Met proteins of EFm1_{D166Q} (10 mg/mL) were crystallized under the same conditions. All of the crystals grew to full size in a week and were flash frozen in liquid nitrogen with an additional 10% glycerol as a cryo-protectant before X-ray diffraction. Crystallographic phases were determined by single-wavelength anomalous diffraction methods from data collected on crystals of Se-Met EFm1_{D166Q} and EFm1_{166–237 aa}. All datasets were obtained at beamlines BL17U1 and BL19U1

at the Shanghai Synchrotron Radiation Facility (SSRF). The collected frames were processed and scaled using the XDS data processing package [21] and HKL2000 [22]. The Se-Met sites and density modification were identified by the HySS tool in phenix package and Resolve, respectively. An initial model was built and refined by Resolve in phenix.autobuild and phenix.refinement, respectively. The final model was built in COOT [23] and refined in Phenix2 [24].

2.5. Lytic Activity Experiment

The lytic activities of wild-type EFm1 and different variants were measured through plate lysis assays and the bacterial growth curve. In the plate lysis assay, wild-type EFm1 and different mutants (2×10^{-7} mol/L, 2 μ L) were dropped onto a BHI semisolid culture medium containing *E. faecalis* 002 in the logarithmic phase, and the plates were observed after 12 h. In the bacterial growth curve assays, a starter culture was prepared using a colony from a freshly inoculated BHI agar plate to inoculate 5 mL of BHI medium. After overnight cultivation, the bacteria were inoculated into 10 mL of BHI medium at a ratio of 1:100 and incubated at 37 °C with shaking (220 rpm/min) until the OD_{600 nm} reached 0.1. The bacterial culture was centrifuged at 8000 \times g for 7 min at room temperature and resuspended in an equal volume of BHI medium. Buffer A was used as a negative control, and 200 μ L of 002 was mixed with 2 μ L of 2×10^{-7} mol/L wild-type EFm1 (positive control) or different mutants. OD_{600 nm} measurements were performed using a BioTek Cytation 5 Cell Imaging Multi-Mode Reader in a 96-well plate every 15 min for 12 h.

To determine the influence of metal ions (Ca²⁺, Cu²⁺, Fe²⁺, Ni²⁺, Mg²⁺ and Zn²⁺) and ethylene diamine tetraacetic acid (EDTA)—a chelating agent combined with divalent metal ions—on the lytic activity of EFm1, 200 μ L of *E. faecalis* 002 was mixed with 1 mM (final concentration) metal ion or EDTA and 2 μ L of 2×10^{-7} mol/L EFm1, and the OD_{600 nm} was measured every 15 min for 12 h. All the growth curves were repeated three times.

2.6. CRISPR Interference Experiments

pDL278-*efm1* was transformed into 002 by electrotransformation, and positive clones were screened from a BHI plate supplemented with 500 μ g/mL spectinomycin. The fresh clones were cultured in BHI medium until the logarithmic growth phase (OD_{600 nm} = 0.1). The bacteria were harvested by centrifugation at 8000 \times g for 7 min and resuspended in equal volumes. Bacteria containing pDL278-sgRNA-dCas9 plasmid were infected with phages at a multiplicity of infection (MOI) of 0.1. The OD_{600 nm} was measured by a BioTek Cytation 5 Cell Imaging Multi-Mode Reader in a 96-well plate every 15 min for 5 h.

2.7. Statistical Analysis and Figure Preparation

The growth curve data are represented as means \pm s.e.m. All figures were produced with PyMOL [25] and GraphPad Prism 8 [26].

3. Results

3.1. Lytic Activity of EFm1

EFm1 was expressed in *E. coli* BL21(DE3) from the pGEX-6P-1 plasmid and then purified. The SDS-PAGE results showed two bands which were further identified approximately 27 kDa and 8 kDa by mass spectrometric analyses (Figure 1A).

The results of the growth curve analysis showed that EFm1 could significantly inhibit the growth of *E. faecalis* 002, ATCC29212, and V583 until 9 h, in contrast to *E. coli* BL21(DE3) and *B. subtilis* CU1050 (Figure 1B–D). There was a slight lag in the growth of *E. faecalis* 002 compared with V583 and ATCC29212 (Figure 1B). These results indicated that EFm1 can specifically lyse *E. faecalis* 002, ATCC29212, and V583 but not *E. coli* BL21(DE3) and *B. subtilis* CU1050.

To further analyze and compare the lytic spectrum of wild-type EFm1 and EFm1^{D166Q}, 23 clinically isolated strains of *E. faecalis* (002, 19, 255, 281, 284, 285, 410, 436, 462, 620, 630,

673, 697, 850, 863, 945, 1550, 1590, 1591, 1592, 1593 and 1763) were used for the plate lysis assay. The results showed that the lytic spectrum of EFm1_{D166Q} was the same as that of wild-type EFm1, and both of them can lyse 22 tested *E. faecalis* clinical strains, except for *E. faecalis* 945.

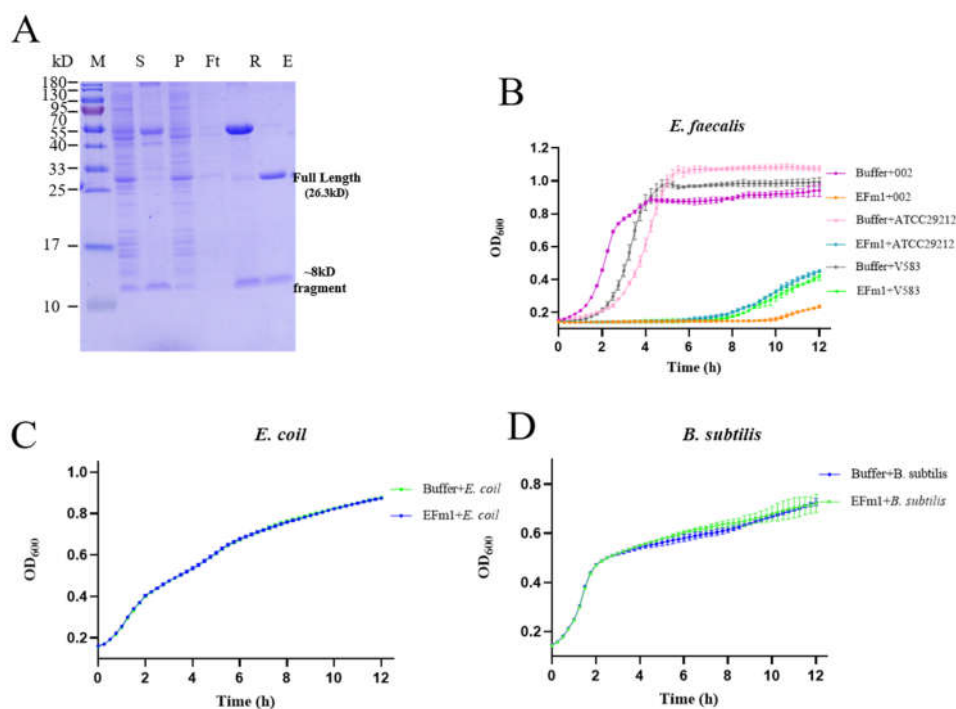


Figure 1. Expression and lytic activity of EFm1. (A) SDS-PAGE analysis of EFm1 expression. S, P, Ft, E and R represent supernatant, pellet, flow through, elution and resin, respectively; (B) The growth curves of 002, ATCC29212 and V583 after adding EFm1; the mean \pm s.e.m is shown; (C) The growth curves of *E. coli* BL21(DE3) after adding EFm1; the mean \pm s.e.m is shown; (D) The growth curves of *B. subtilis* CU1050 after adding; the mean \pm s.e.m is shown.

3.2. Structures of EFm1_{D166Q} and EFm1_{166–237 aa}

The structures of EFm1_{D166Q} and EFm1_{166–237 aa} were determined to elucidate the molecular mechanism; the structure of EFm1_{D166Q} was successfully determined at 2.2 Å resolution in the P12₁ space group by X-ray crystallography. The structure of C-terminal EFm1 was refined at 2.0 Å in the I4₁22 space group. EFm1_{D166Q} contains an NTD (1–145 aa), a CTD (165–237 aa) and a linker (145–165 aa) (Figure 2A). A CHAP domain is located in the NTD and the CTD forms a tetramer. The linker connects the NTD and CTD.

Similar to the lysin PlyC from *streptococcal* specific phage, of which CTDs are arranged in a planar octameric ring [27], the CTDs of EFm1_{D166Q} also are arranged in a planar tetrameric ring consisting of a CTD of full-length EFm1_{D166Q} and three CTDs (Figure 2B). The final refined structure of EFm1_{D166Q} possessed good stereochemistry except for residues 145–165, where the electron density was missing due to its high flexibility. The CHAP domain of EFm1_{D166Q} is composed of three α -helices, two 3_{10} -helices and six β -strands (Figure 2B). Two α -helices are interconnected by a long loop (L1, 14–29 aa). Together, this loop and its neighbor loop (L2, 108–123 aa) form negative potential on the surface of the protein (Figure 2C). A hydrophobic groove is formed between the two loops and the two 3_{10} -helices (Figure 2C). This arrangement might contribute to the catalytic activity responsible for the cleavage of peptidoglycan bonds.

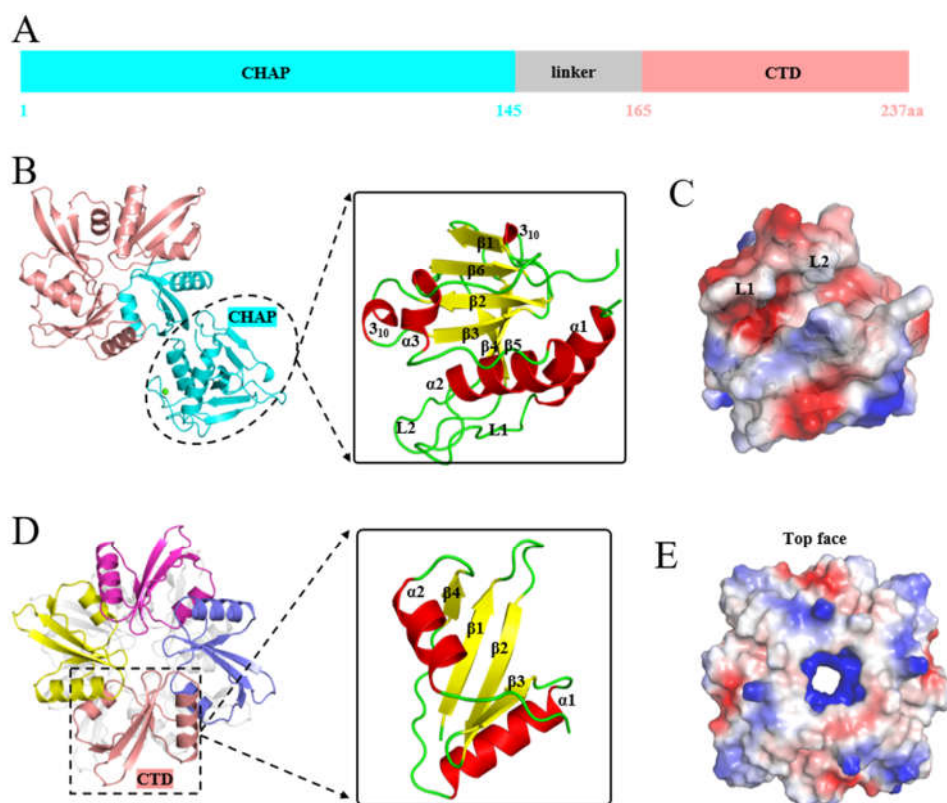


Figure 2. Three-dimensional structures of EFm1_{D166Q} and EFm1_{166–237 aa}. (A) Domain organization of EFm1; (B) Structure of EFm1_{D166Q} including the NTD (1–165 aa), the CTD (165–237 aa) and a putative linker (145–165 aa); (C) Electron density maps of the CHAP domain; (D) Structure of EFm1_{166–237 aa}; (E) Electron density map of EFm1_{166–237 aa}.

The structure of EFm1_{166–237 aa} is the same as the C-terminal domain of the refined EFm1_{D166Q} (Figure 2D). The structure of EFm1_{166–237 aa} shows eight monomers in an asymmetric unit. However, extensive intermonomer interfaces occur only in every four monomers in the crystal, suggesting that in solution, the protein is tetrameric. Each monomer is composed of a four-stranded β -sheet capped on each side by a short α -helix, which is arranged in the characteristic α - β - α fold. The four β -strands together form the central β -sheet layer of EFm1-CTD. The “sandwich” conformation greatly stabilizes tetramerized EFm1. Notably, this tetramer structure maximizes the arrangement of internal hydrophilic residues and external hydrophobic residues with the formation of internal positively charged cavities (Figure 2E). Together, these results imply that the tetramerized EFm1-CTD might be crucial for phage anchoring on the peptidoglycan. The crystal data are shown in Table 2.

Table 2. Data and refinement statistics.

Property	EFm1 _{D166Q}	CTD
Space group	I 41 2 2	I 41 2 2
Cell constants	46.87 Å 57.26 Å 91.27 Å	115.59 Å 115.59 Å 179.72 Å
a, b, c, α , β , γ	90.00° 96.57° 90.00°	90.00° 96.57° 90.00°
Resolution (Å)	48.46–2.20	49.73–2.00
	48.42–2.20	49.68–2.00
% Data completeness	99.9 (48.46–2.20)	99.0 (49.73–2.00)
(in resolution range)	98.2 (48.42–2.20)	98.2 (49.68–2.00)

R_{merge}	0.00	0.00
$\langle I/\sigma(I) \rangle$	2.75 (at 2.20 Å)	1.39 (at 2.00 Å)
Refinement program	REFMAC 5.8.0267, REFMAC 5.8.0267	REFMAC 5.8.0267, REFMAC 5.8.0267
R , R_{free}	0.179, 0.215	0.183, 0.216
	0.197, 0.223	0.177, 0.214
R_{free} test set	1295 reflections (5.27%)	1998 reflections (4.91%)
Wilson B-factor (Å)	27.1	21.8
Anisotropy	0.681	0.121
Bulk solvent k_{sol} (e/Å), B_{sol} (Å)	0.39, 33.6	0.42, 58.0
L-test for twinning	$\langle L \rangle = 0.49$, $\langle L^2 \rangle = 0.32$	$\langle L \rangle = 0.49$, $\langle L^2 \rangle = 0.32$
Estimated twinning fraction	No twinning to report.	No twinning to report.
F_o , F_c correlation	0.94	0.96
Total number of atoms	6953	9609
Average B, all atoms (Å)	24.0	23.0

Statistics for the highest-resolution shell are shown in parentheses.

3.3. The Effect of the NTD, CTD and Linker on the Lytic Activity of EFm1

To assess the effect of the NTD, CTD and linker on the lytic activity of EFm1, we expressed the NTD, CTD and mutant lacking the linker (Figure 3A). SDS-PAGE of the mutant lacking the linker showed only a band slightly lower than that of wild-type EFm1. Therefore, we hypothesize that amino acids located at approximately residues 145–165 are responsible for generating the 8 kDa fragment. The growth curves and plate lysis assay showed that the NTD, CTD and mutant lacking the linker showed no lytic activity compared with wild-type EFm1 (Figure 3B,C). This indicated that only full-length EFm1 could lyse *E. faecalis*.

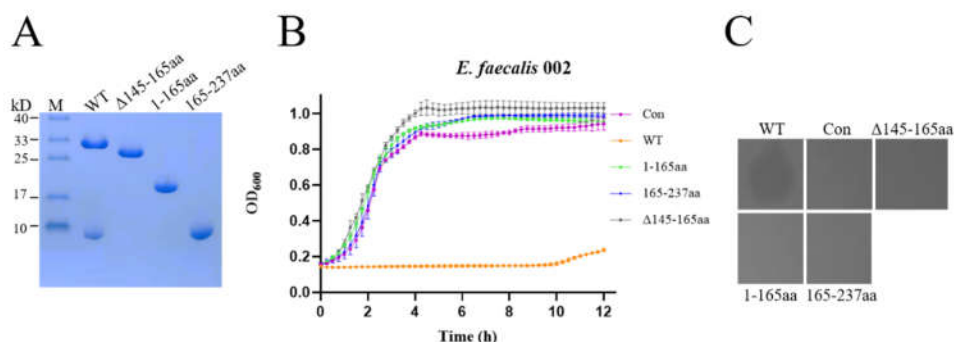


Figure 3. Expression and lytic activity of the EFm1 domains. (A) SDS-PAGE results of the EFm1 domain; (B) Growth curves of the EFm1 domains; the mean \pm s.e.m is shown; (C) Plate lysis assay results of the EFm1 domain.

3.4. Binding Sites and Iron Channel of EFm1

To identify the region of the EFm1 tetramer that is involved in cell wall binding, we undertook a mutagenesis study, mutating residues in the concave region of EFm1. There was a prominent convex region in each monomer that was lined by residues K173, K176, R190 and K236, resulting in a positively charged patch surrounding the convex (Figure 4A). Thus, we hypothesize that the convex positively charged interface forms a site for binding the bacterial cell wall through ionic bonds. To verify the involvement of binding sites in this positively charged patch, we mutated residues K173, K176, R190 and K236 to glutamic acid. None of these mutations interfered with the formation of the EFm1 tetramer ring or the formation of the holoenzyme (Figure 4B). The results of growth curve and plate lysis assays indicated that the K173E, K176E and K236E mutants retained lytic activity, while the R190E mutant showed no lytic activity compared to wild-type EFm1.

We hypothesize that R190 is the key residue mediating binding between EFm1 and *E. faecalis* (Figure 4C,D).

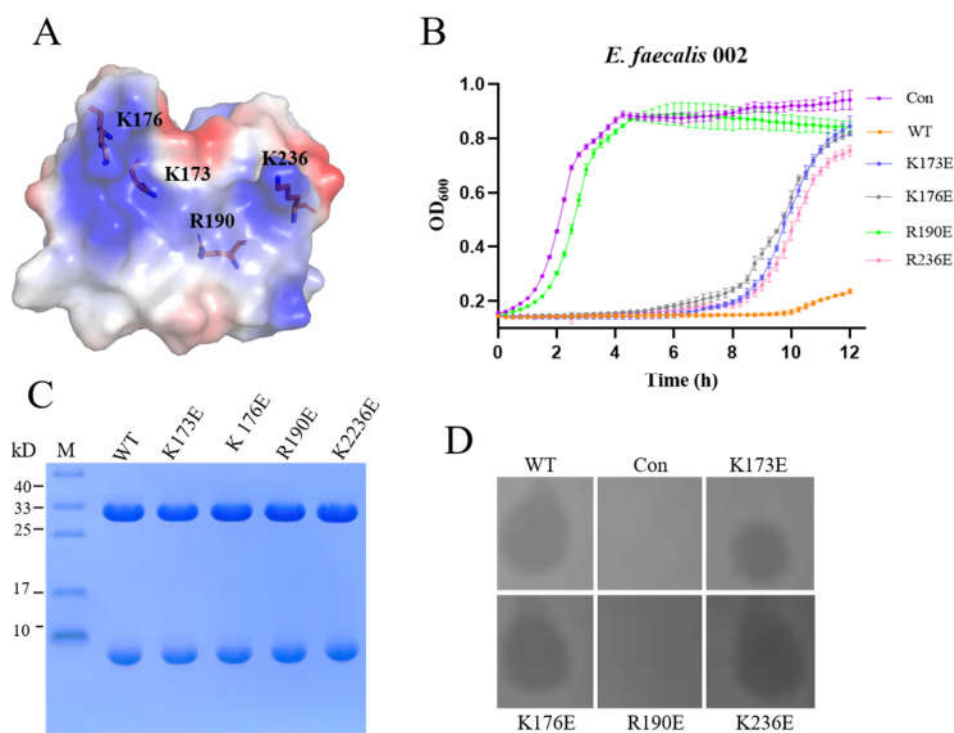


Figure 4. The binding sites of EFm1 for cell wall. (A) Residues with a positive charge in the convex region of the monomer; (B) Growth curves of the mutants K173E, K176E, R190E and K236E; the mean \pm s.e.m is shown; (C) SDS-PAGE results of the mutants K173E, K176E, R190E and K236E; (D) Plate lysis assay results of the mutants K173E, K176E, R190E and K236E.

3.5. Lytic Activity of the CHAP Domain of EFm1

Similar to LysGH15 (PDB: 4OLK) and LysK (PDB: 4CSH), the CHAP domain of EFm1 contains a calcium ion which coordinates with the conserved residues D20, D22, W24, G26, and D31 and one water molecule (Figure 5A). The growth curves showed that there was no activity when EDTA was mixed with EFm1, while activity was restored after the addition of calcium, indicating that calcium is important during lysis (Figure 5B).

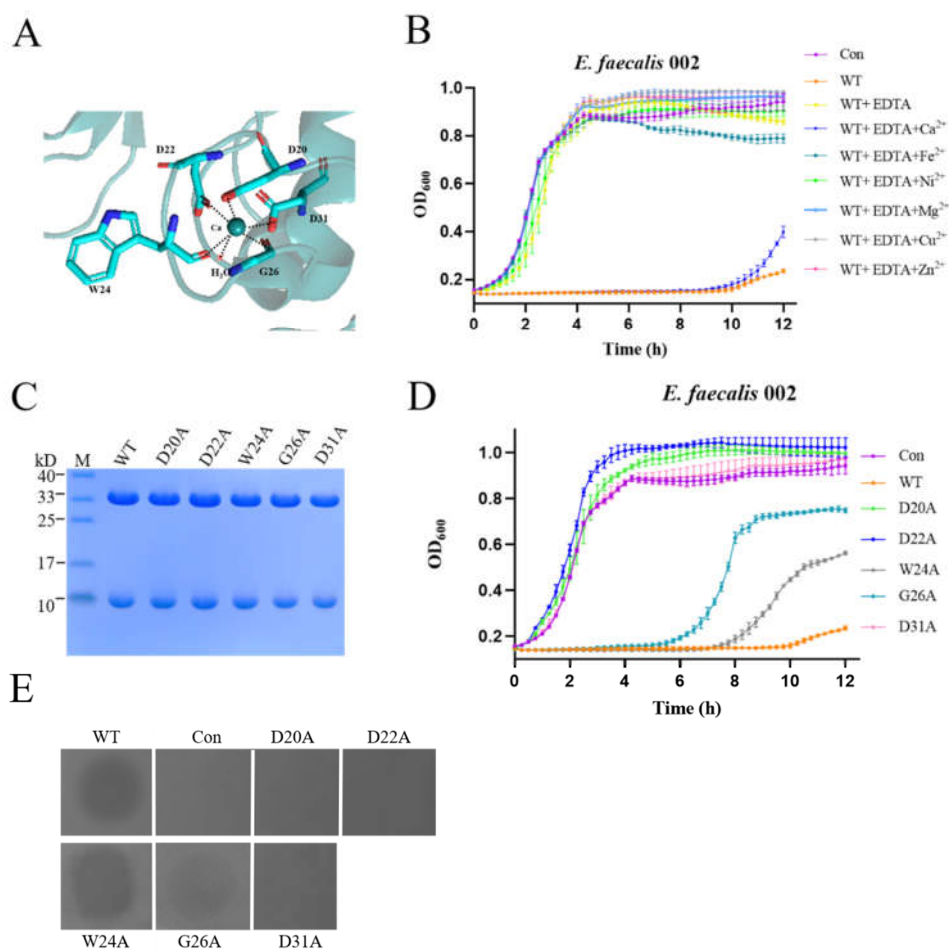


Figure 5. Effect of calcium on the lytic activity of EFm1. (A) Residues coordinating with calcium; (B) Effects of different metal ions (1 μ M) on the lytic activity of EDTA-inactivated EFm1; the mean \pm s.e.m is shown; (C) SDS-PAGE results of mutants coordinated with calcium; (D) Growth curves of mutants coordinated with calcium; the mean \pm s.e.m is shown; (E) Plate lysis assay results of mutants coordinated with calcium.

Eijsink et al. suggested that protease easily recruit metal ions to the active center in the calcium-rich environment of gram-positive cells; the stable states of protease are regulated by the number of calcium binding sites [28]. When all calcium binding sites are occupied, protease can fold to a stable, active conformation. Therefore, calcium usually serves as a switch to regulate the activity of proteases. As such, atoms coordinating with calcium could affect the activity of proteases by changing the spatial position of calcium, such as subtilisin or alpha-lytic protease [28]. Like LysGH15 [29], the mutants W24A and G26A of EFm1 remained active, while mutations at D20, D22 and D31 abolished activity (Figure 5C–E).

Besides calcium, there is a putative classic amidohydrolase catalytic triad consisting of residues C29, H90 and D108 in CHAP (Figure 6A). The putative catalytic triad is clearly next to the calcium, and a 2.8 Å distance was observed between H90 and D108. In addition, C29 and H90 are located in the cleft of the CHAP domain. The growth curves and plate lysis assay showed that there was no lytic activity among the C29A, H90A and D108A mutants (Figure 6B,D). Shin et al. reported that the nucleophilic residue (Ser or Cys) is most likely in the protonated form at physiological pH [30]. The nucleophile is maintained

in the deprotonated state by the direct hydrogen-bonding interactions provided by the side-chain-NH and the side-chain-OH groups from acidic amino acids and basic amino acids, respectively. Then, nucleophilic attack by the nucleophile on the carbonyl carbon of the substrate results in the cleavage and formation of chemical bonds [30]. The three residues (C29, H90 and D108) forming the putative catalytic triad affect the lytic activity. It is possible that D108 bonds with H90 by hydrogen bonding, causing C29 deprotonation, which cleaves the chemical bonds in peptidoglycan. Therefore, calcium may also regulate protein activity by regulating C29 to place it in the correct spatial orientation, and coordinates with a putative classic amidohydrolase catalytic triad to contribute to the activity of EFm1.

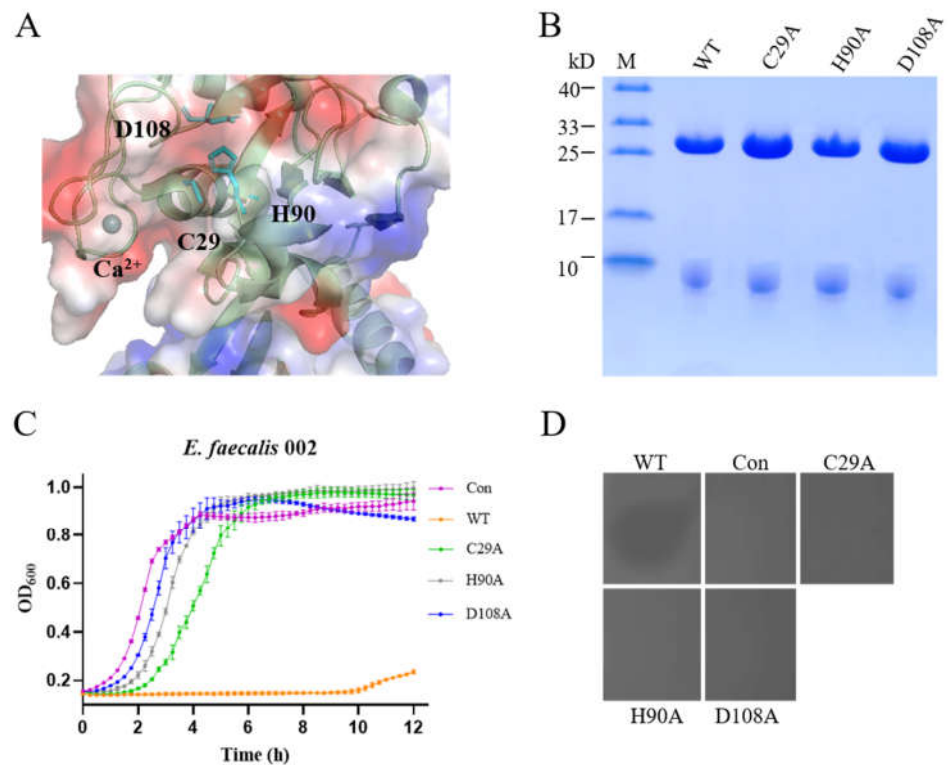


Figure 6. Lytic activity of the amidohydrolase catalytic triad (C29, H90 and D108) in EFm1. (A) Structure of the amidohydrolase catalytic triad; (B) SDS-PAGE results of mutants with amidohydrolase catalytic triad; (C) Growth curves of mutants with amidohydrolase catalytic triad; the mean \pm s.e.m is shown; (D) Plate lysis assay results of mutants with amidohydrolase catalytic triad.

3.6. Lytic Activity of the Tetramer of EFm1

We found that there was only one protein band for the mutant lacking the linker (Figure 3A), so we hypothesized that amino acids located at approximately residues 145–165 were responsible for generating the 8 kDa fragment. After analyzing the sequence of *efm1*, we hypothesized that M168 acted as an alternative start codon for in-frame translation. The mutant M168A peak appeared later than the wild-type EFm1 peak in the size-exclusion chromatography experiment (Figure 7B), and the 8 kDa band disappeared (Figure 7C). The above results indicated that M168 is responsible for the translation of the 8 kDa fragment.

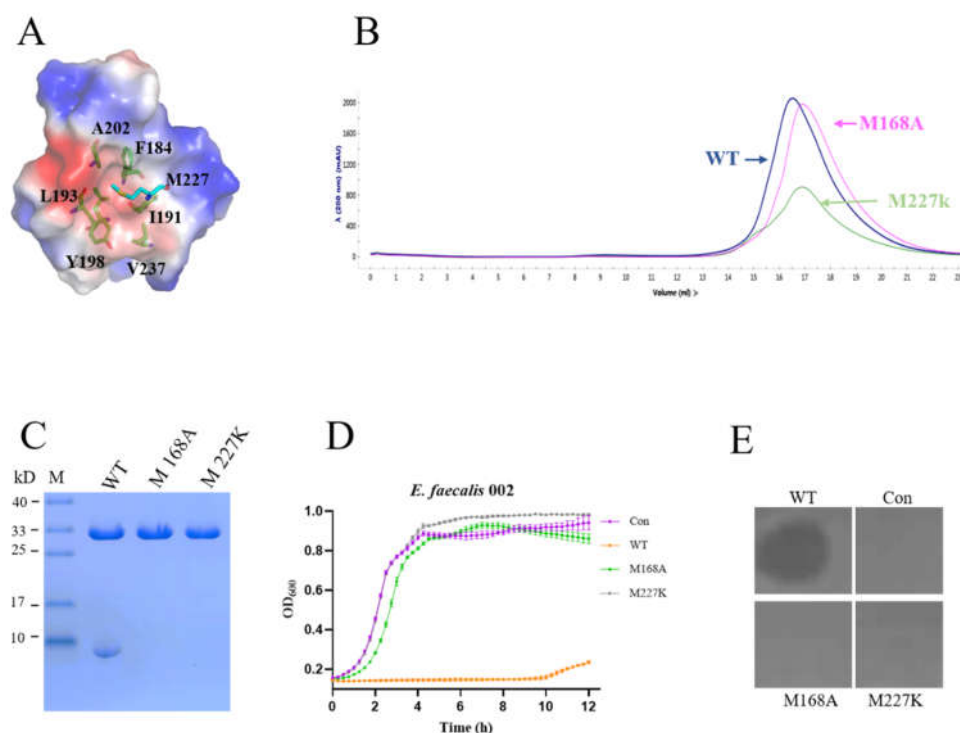


Figure 7. Lytic activity of the EFm1 tetramer. (A) Hydrophobic interactions between M227 and the nearby monomer; (B) Size-exclusion chromatography of WT, M168A and M227K; (C) SDS-PAGE results of the mutants M168A and M227K, respectively; (D) Growth curves and plate lysis assay results of the mutants M168A and M227K, respectively; the mean \pm s.e.m is shown; (E) Plate lysis assay results of the mutants M168A and M227K, respectively.

Next, we tried to reveal the assembly mechanism of the 8 kDa fragment. By structural analysis, we found that M227 was bound to another monomer with a hydrophobic cage composed of F184, I191, L193, Y198, A202 and V237 (Figure 7A). In the size-exclusion chromatography experiment, the mutant M227K peak appeared later than the wild-type EFm1 peak (Figure 7B). By SDS-PAGE analysis, there was only one band at approximately 27 kDa (Figure 7C). The result for the M227A mutant was the same as that for wild-type EFm1 (data not shown), suggesting that recognition and interaction are mediated by hydrophobic interactions between the full-length unit and three additional fragments. The growth curves and plate lysis assay showed that the M168A and M227K mutants had no lytic activity, confirming that oligomeric tetramerization of EFm1 is essential for its lytic activity (Figure 7D,E).

3.7. Interaction of the Monomer and Ion Channel in the CTD

We know that there is a strong hydrophobic interaction between monomers and a large amount of hydrogen bonding. Structural analysis showed the presence of some hydrogen bonds between residues of the α -helix in one monomer and the β 4-sheet in the adjacent monomer. Residue R208 forms hydrogen bonds with residues Y218 and A231 and residues Y209 and F169 of the adjacent protomer (Figure 8A). To assess the importance of these residues for tetramerization and activity, we constructed variants of EFm1. SDS-PAGE showed that R208A and Y209A did not interfere with the formation of the holoenzyme (Figure 8C), while the plate lysis assay showed that these variants were not active (Figure 8D).

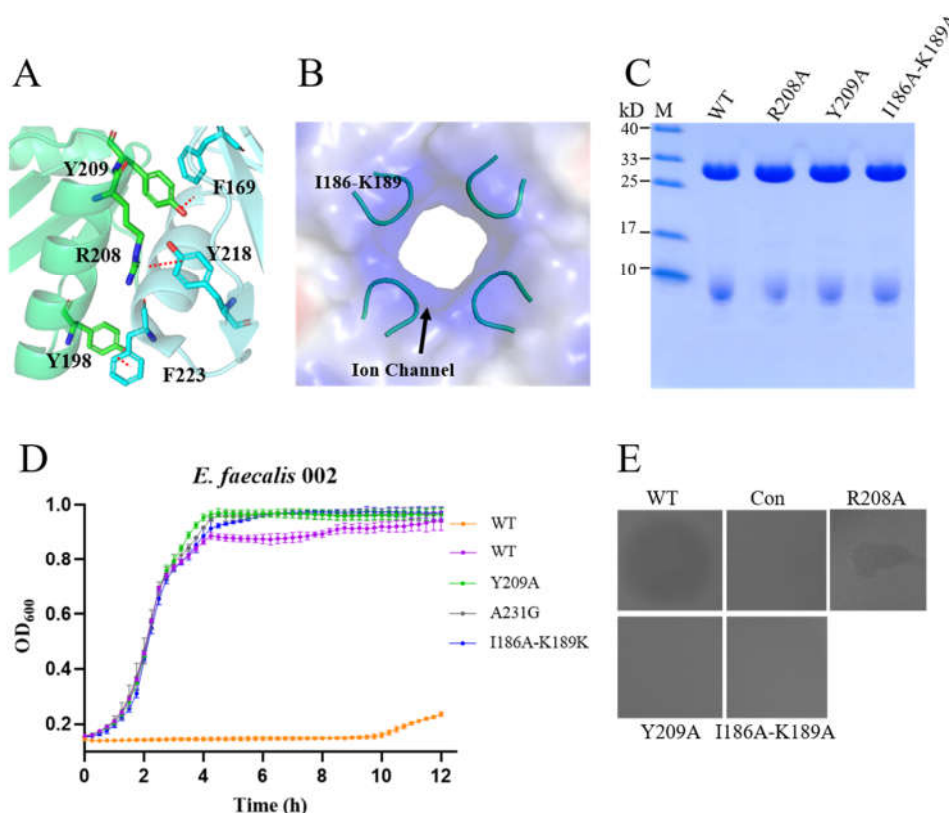


Figure 8. Putative ion channel and interaction between EFm1 monomers. (A) Putative ion channel in the CTD of EFm1; (B) The interaction between monomers of EFm1; (C) SDS-PAGE results of the mutants R208A, Y209A and I186A-K189A, respectively; (D) Growth curves of the mutants R208A, Y209A and I186A-K189A, respectively; the mean \pm s.e.m is shown; (E) Plate lysis assay results of the mutants R208A, Y209A and I186A-K189A, respectively.

There is a putative iron channel (I186-K189) in the CTD of EFm1 (Figure 8B) which was filled with positively charged residues. SDS-PAGE showed that this four-residue mutation did not interfere with the formation of the holoenzyme (Figure 8B), while the plate lysis assay showed that the mutants were not active (Figure 8D).

All the domains and residues identified in this study are summarized in Table 3.

Table 3. Summary of the domains and residues identified as being important for the stability and lytic activity of EFm1 in this study.

Structural Characteristics	Mutants	Stability	Lytic Activity
Critical domains	NTD (1–165 aa)	–	–
	CTD (165–237 aa)	–	–
	EFm1 lacking the linker (Δ 145–165 aa)	–	–
Putative residues binding to the host cell	K173E	+	+
	K176E	+	+
	R190E	+	–
	K236E	+	+
Residues binding calcium	D20A	+	–
	D22A	+	–
	W24A	+	+
	G26A	+	+
	D31A	+	–
Residues forming a putative catalytic triad	C29A	+	–

	H90A	+	–
	D108A	+	–
Residues producing and assembling the 8 kDa fragment	M168A	–	–
	M227K	–	–
Residues forming the interaction surface	R208A	+	–
	Y209A	+	–
Residues forming the putative ion channel	I186A-K189A	+	–

Note: + and – in the stability column indicate the presence and absence of the 8 kDa protein band, respectively. In the lytic activity column, + indicates that the mutant had lytic activity toward 002, and – indicates that the mutant had no lytic activity toward 002.

3.8. Expression In Vivo and Knockdown of EFm1 in 002

The growth of 002 containing the plasmid pDL278-*efm1* was measured to investigate the lytic activity of EFm1 in vivo. From 3 h to 6 h, the growth of 002 containing the plasmid pDL278-*efm1* was slightly lower than that of the control (Figure 9A). After that, the growth dynamics of the two strains were similar. These results implied that EFm1-mediated lysis in the IME-EF may need holins for better activity.

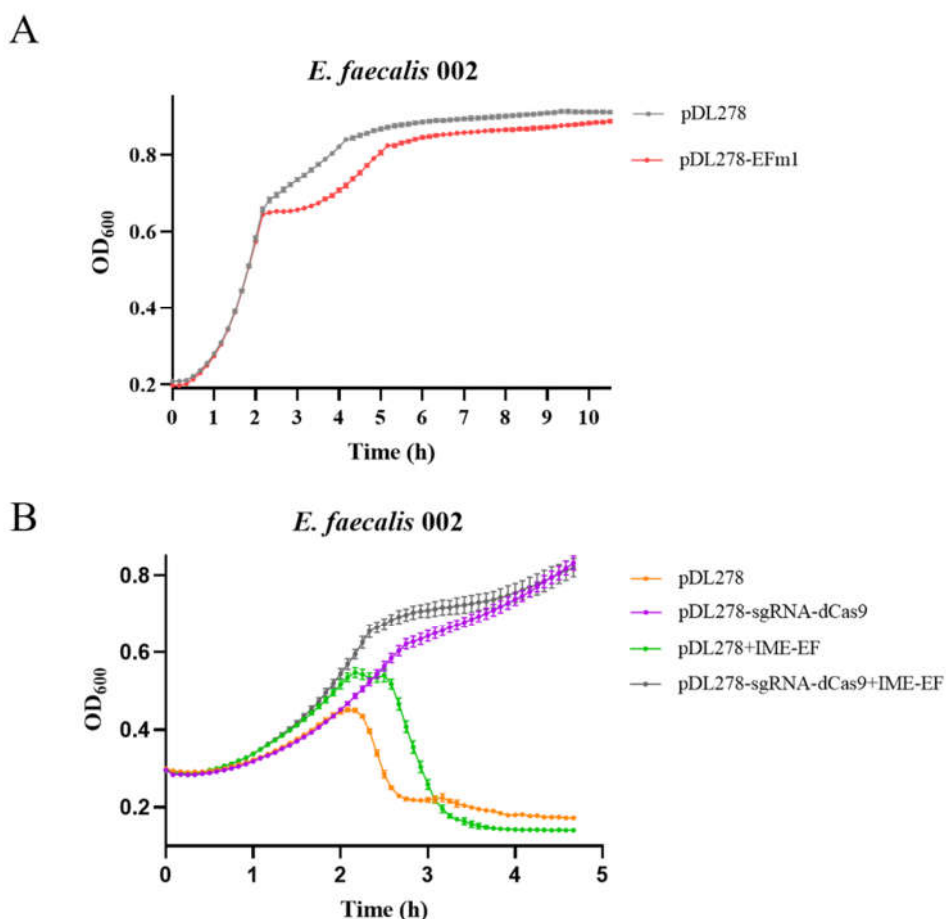


Figure 9. Expression and CRISPRi of EFm1 in 002. (A) Growth dynamics of 002 with the plasmid pDL278 or pDL278-*efm1*; the mean \pm s.e.m is shown; (B) Growth dynamics of 002 with the plasmid pDL278 or pDL278-dCas9-sgRNA followed by infection without or with the phage IME-EF1 (MOI = 0.1); the mean \pm s.e.m is shown.

In addition, we carried out a CRISPRi experiment to investigate whether silencing of *efm1* affected the activity of phage during infection (Figure 9B). The growth curves showed that from 2 h to 3 h, the growth of 002 containing pDL278-dCas9-sgRNA and infected with the phage IME-EF1 was higher than that of 002 containing pDL278 and infected with the phage IME-EF1, indicating that silencing *efm1* resulted in a decrease in the lytic activity of the phage IME-EF1 toward 002.

4. Discussion

The aims of this study were to investigate the lytic spectrum of EFm1 toward *E. faecalis*, identify the crucial domains and residues affecting the lytic activity of EFm1 and analyze the role of EFm1 in phage IME-EF1 infection. Based on a structural analysis, bacterial growth curves and plate lysis assays further identified some domains and novel residues that were important for the stability and lytic activity of EFm1, such as the NTD, CTD, linker, residues involved in host cell-binding sites, calcium-binding sites, the putative catalytic triad, 8 kDa assembly fragment, surface interaction sites and ion channel sites.

To analyze the lytic spectrum of EFm1, which specifically lyses *E. faecalis*, we tested its lytic ability against clinically isolated strains. EFm1 and EFm1_{D166Q} could lyse 22 clinical strains, except *E. faecalis* 945. We hypothesized that *E. faecalis* 945 may possess a unique capsule or biofilm or a hydrolase on the outer cell wall, helping it escape or resist the activity of EFm1, or absent tail fiber protein of phage which specifically degrades biofilm during the phage host interaction [31]. These implied that *E. faecalis* 945 might be the most suitable bacteria used to further investigate the resistance mechanisms of endolysins and the emergence of endolysin-resistant *E. faecalis* might bring new challenge for phage therapy.

In this research, the structure of EFm1_{D166Q} showed that there are three domains (a CTD, an NTD and a putative linker) in the holoenzyme. CHAP and calcium- or cell wall-binding domains are present at the N-terminus and C-terminus, respectively. Crystal data and biochemical experiments revealed that EFm1 contains four potential binding sites (R190) in the convex region of CTDs for cell wall components which may allow tighter, more stable interactions to occur between the holoenzyme and the cell wall, in contrast to most lysins containing only a single CBD [27,32]. However, we are not sure if all four binding sites simultaneously participate in coordinating holoenzyme binding to cell wall.

The results showed that there was no lytic activity when mutate residues coordinating calcium with were present in the side groups or formed putative classic amidohydrolase catalysts. In the highly conserved triad, the protonation of the nucleophilic residue by acid/base glutamate facilitates the first step of the catalytic reaction [33]. We speculate that lysis proceeds as follows: calcium regulates C29 to ensure the correct spatial orientation, and the -NH of H90 interacts with the -OH of D108, leading to the deprotonation of C29. Next, the highly flexible linker undergoes a conformational change to allow the N-terminus to reach the surface of the cell wall. Finally, the deprotonated C29 attacks the carbonyl carbon of the substrate, resulting in the cleavage of the chemical bonds of peptidoglycan.

M168, an alternative start codon for in-frame translation, is responsible for the generation of the other three fragments [16]. We have found that M227 inserting a hydrophobic pocket in the adjacent monomer is crucial to assemble the tetramer. Ortega et al. reported that NisB substrate recognition and interaction is mediated by hydrophobic interactions between NisB and NisA [34]. As such, multiple novel residues identified with different structural characteristics may affect the lytic activity of EFm1.

In this research, some of our results are consistent with those reported by Zhou et al. [16], such as the effects of residues C29, H90, M168, R190 or EDTA on the lytic activity of EFm1. Furthermore, some novel residues affecting the lytic activity of EFm1 were identified in this study. For example, although Zhou et al. reported that N110 was one of residues forming a putative catalytic triad, we found that residue D108 might also form the

putative catalytic triad. Furthermore, we have proved that residues D20, D22 and D31 coordinated with calcium in its side groups or located between monomers R208 and Y209 were the key sites of activity. We also found that the hydrophobicity of M227 was responsible for the tetramer.

EFm1 exhibited no significant activity when expressed alone in vivo, and CRISPRi showed that 002 had a slight resistance to IME-EF when *efm1* was silenced. It is reported that holins make a hole in the bacterial cytoplasmic membrane to create a channel to help lysin delivery to the peptidoglycan and the release of phage progeny at the end of the lytic cycle [11,35,36]. It is possible that EFm1 cannot be effectively released in the absence of holins.

5. Conclusions

This research further expands the lytic spectrum of EFm1 to *E. faecalis*. It also identified the EFm1-resistant strain *E. faecalis* 945, obtained the structures of EFm1_{D166Q} and EFm1_{166–237aa}, identified novel crucial residues affecting the lytic activity of EFm1, and analyzed their role in phage infection. Notably, we could not clearly explain why the electron density in the linker loop was missing. Additionally, the cleavage mechanism of EFm1 needs further research. Further investigation of EFm1 will be important not only to elucidate the working mechanism of EFm1 but also to promote research into the preparation of functional biomaterials based thereon. This study provides a research basis for EFm1, which is becoming recognized as a new generation of antibacterial biomaterial and a viable choice for the treatment of diseases caused by the opportunistic pathogen *E. faecalis*.

Author Contributions: Conceptualization, W.C. and X.Z. (Xuerong Zhou); methodology, X.Z. (Xuerong Zhou) and L.W.; resources, X.Z. (Xuerong Zhou), X.Z. (Xiaotao Zeng), G.Z. (Guixiang Zhang) and L.W.; data curation, X.Z. (Xuerong Zhou), X.Z. (Xiaotao Zeng), L.W. and Y.Z. (Yanhui Zheng); writing—original draft preparation, X.Z. (Xuerong Zhou), X.Z. (Xiaotao Zeng), G.Z., Y.Z. and W.C.; writing—review and editing, X.Z. (Xuerong Zhou), X.Z. (Xiaotao Zeng), G.Z. and W.C. All authors have read and agreed to the published version of the manuscript.

Funding: This research was funded by grants from the National Natural Science Foundation of China (31870836 and 32071236) and the 1.3.5 Project for Disciplines Excellence of West China Hospital, Sichuan University (ZYYC20005).

Institutional Review Board Statement: Not applicable.

Informed Consent Statement: Not applicable.

Data Availability Statement: Data are available on request to the authors.

Acknowledgments: We thank Yi-Gang Tong for providing the *E. faecalis* strains and *E. faecalis* phage IME-EF1 and Xiao-Jing Huang for providing V583. We thank Qin Su and Li Cheng for providing ATCC29212 and plasmid pDL278, respectively. We thank the staff of the BL17U1 beamline and BL19U1 at the Shanghai Synchrotron Radiation Facility for assistance during data collection.

Conflicts of Interest: The authors declare no conflict of interest.

References

1. Holmes, A.H.; Moore, L.S.; Sundsfjord, A.; Steinbakk, M.; Regmi, S.; Karkey, A.; Philippe, J.G.; Piddock, L.J. Understanding the mechanisms and drivers of antimicrobial resistance. *Lancet* **2016**, *387*, 176–187. [https://doi.org/10.1016/S0140-6736\(15\)00473-0](https://doi.org/10.1016/S0140-6736(15)00473-0).
2. Song, M.; Liu, Y.; Huang, X.; Ding, S.; Wang, Y.; Shen, J.; Zhu, K. A broad-spectrum antibiotic adjuvant reverses multidrug-resistant gram-negative pathogens. *Nat. Microbiol.* **2020**, *5*, 1040–1050. <https://doi.org/10.1038/s41564-020-0723-z>.
3. Pöntinen, A.K.; Top, J.; Arredondo-Alonso, S.; Tonkin-Hill, G.; Freitas, A.R.; Novais, C.; Gladstone, R.A.; Pesonen, M.; Meneses, R.; Pesonen, H.; et al. Apparent nosocomial adaptation of *Enterococcus faecalis* predates the modern hospital era. *Nat. Commun.* **2021**, *12*, 1–13. <https://doi.org/10.1038/s41467-021-21749-5>.
4. Yang, H.; Singh, M.; Kim, S.J.; Schaefer, J. Characterization of the tertiary structure of the peptidoglycan of *Enterococcus faecalis*. *Biochim. Biophys. Acta* **2017**, *1859*, 2171–2180. <https://doi.org/10.1016/j.bbamem.2017.08.003>.

5. Yoon, Y.K.; Sim, H.S.; Kim, J.Y.; Park, D.W.; Sohn, J.W.; Roh, K.H.; Lee, S.E.; Kimm, M.J. Epidemiology and control of an outbreak of vancomycin-resistant *enterococci* in the intensive care units. *Yonsei Med. J.* **2009**, *50*, 637–643. <https://doi.org/10.3349/ymj.2009.50.5.637>.
6. Sabbagh, P.; Rajabnia, M.; Maali, A.; Ferdosi-Shahandashti, E. Integron and its role in antimicrobial resistance: A literature review on some bacterial pathogens. *Iran. J. Basic Med. Sci.* **2021**, *24*, 136–142. <https://doi.org/10.22038/ijbms.2020.48905.11208>.
7. Hegstad, K.; Mikalsen, T.; Coque, T.M.; Werner, G.; Sundsfjord, A. Mobile genetic elements and their contribution to the emergence of antimicrobial resistant *Enterococcus faecalis* and *Enterococcus faecium*. *Clin. Microbiol. Infect.* **2010**, *16*, 541–554. <https://doi.org/10.1111/j.1469-0691.2010.03226.x>.
8. Biswas, B.; Adhya, S.; Washart, P.; Paul, B.; Trostel, A.N.; Powell, B.; Carlton, R.; Merrill, C.R. Bacteriophage therapy rescues mice bacteremic from a clinical isolate of vancomycin-resistant *Enterococcus faecium*. *Infect. Immun.* **2002**, *70*, 204–210. <https://doi.org/10.1128/IAI.70.1.204-210.2002>.
9. Fischetti, V.A. Bacteriophage endolysins: A novel anti-infective to control Gram-positive pathogens. *Int. J. Med. Microbiol.* **2010**, *300*, 357–362. <https://doi.org/10.1016/j.ijmm.2010.04.002>.
10. Gondil, V.S.; Harjai, K.; Chhibber, S. Endolysins as emerging alternative therapeutic agents to counter drug-resistant infections. *Int. J. Antimicrob. Agents* **2020**, *55*, 105844. <https://doi.org/10.1016/j.ijantimicag.2019.11.001>.
11. Chang, Y. Bacteriophage-derived endolysins applied as potent biocontrol agents to enhance food safety. *Microorganisms* **2020**, *8*, 724. <https://doi.org/10.3390/microorganisms8050724>.
12. Gu, J.; Xi, H.; Cheng, M.; Han, W. Phage-derived lysins as therapeutic agents against multidrug-resistant *Enterococcus faecalis*. *Future Microbiol.* **2018**, *13*, 275–278. <https://doi.org/10.2217/fmb-2017-0235>.
13. Hathaway, H.; Ajuebor, J.; Stephens, L.; Coffey, A.; Potter, U.; Sutton, J.M.; Jenkins, A.T.A. Thermally triggered release of the bacteriophage endolysin CHAP(K) and the bacteriocin lysostaphin for the control of methicillin resistant *Staphylococcus aureus* (MRSA). *J. Control. Release* **2017**, *245*, 108–115. <https://doi.org/10.1016/j.jconrel.2016.11.030>.
14. Zhang, W.; Mi, Z.; Yin, X.; Fan, H.; An, X.; Zhang, Z.; Chen, J.; Tong, Y. Characterization of *enterococcus faecalis* phage IME-EF1 and its endolysin. *PLoS ONE* **2013**, *8*, e80435. <https://doi.org/10.1371/journal.pone.0080435>.
15. Cheng, M.; Zhang, Y.; Li, X.; Liang, J.; Gu, J. Endolysin LysEF-P10 shows potential as an alternative treatment strategy for multi-drug-resistant *Enterococcus faecalis* infections. *Sci. Rep.* **2017**, *10164*, 1–15. <https://doi.org/10.1038/s41598-017-10755-7>.
16. Zhou, B.; Zhen, X.; Zhou, H.; Zhao, F.; Fan, C.; Perčulija, V.; Tong, Y.; Mi, Z.; Ouyang, S. Structural and functional insights into a novel two-component endolysin encoded by a single gene in *Enterococcus faecalis* phage. *PLoS Pathog.* **2020**, *16*, e1008394. <https://doi.org/10.1371/journal.ppat.1008394>.
17. Dou, C.; Xiong, J.; Gu, Y.; Yin, K.; Wang, J.; Hu, Y.; Zhou, D.; Fu, X.; Qi, S.; Zhu, X.; et al. Structural and functional insights into the regulation of the lysis-lysogeny decision in viral communities. *Nat. Microbiol.* **2018**, *3*, 1285–1294. <https://doi.org/10.1038/s41564-018-0259-7>.
18. Goldschmidt, L.; Cooper, D.R.; Derewenda, Z.S.; Eisenberg, D. Toward rational protein crystallization: A Web server for the design of crystallizable protein variants. *Protein Sci.* **2007**, *16*, 1569–1576. <https://doi.org/10.1110/ps.072914007>.
19. Slabinski, L.; Jaroszewski, L.; Rychlewski, L.; Wilson, I.A.; Lesley, S.A.; Godzik, A. XtalPred: a web server for prediction of protein crystallizability. *Bioinformatics* **2007**, *15*, 3403–3405. <https://doi.org/10.1093/bioinformatics/btm477>.
20. Sun, Q.; Hu, Y.; Gu, Y.; Huang, J.; He, J.; Luo, L.; Yang, Y.; Yin, S.; Dou, C.; Wang, T.; et al. Deciphering the regulatory and catalytic mechanisms of an unusual SAM-dependent enzyme. *Signal Transduct. Target. Ther.* **2019**, *24*, 17. <https://doi.org/10.1038/s41392-019-0052-y>.
21. Wang, Q.; Yu, F.; Huang, S.; Sun, B.; Zhang, K.; Liu, K.; Wang, Z.; Xu, C.; Wang, S.; Yang, L. The macromolecular crystallography beamline of SSRF. *Nucl. Sci. Tech.* **2015**, *26*, 8–13. <https://doi.org/10.13538/j.1001-8042/nst.26.010102>.
22. Zhang, J.; McCabe, K.A.; Bell, C.E. Crystal structures of λ exonuclease in complex with DNA suggest an electrostatic ratchet mechanism for processivity. *Proc. Natl. Acad. Sci. USA* **2011**, *108*, 11872–11877. <https://doi.org/10.1073/pnas.1103467108>.
23. Emsley, P.; Lohkamp, B.; Scott, W.G.; Cowtan, K. Features and development of Coot. *Acta Crystallogr. D Biol. Crystallogr.* **2010**, *66*, 486–501. <https://doi.org/10.1107/S0907444910007493>.
24. Afonine, P.V.; Grosse-Kunstleve, R.W.; Echols, N.; Headd, J.J.; Moriarty, N.W.; Mustyakimov, M.; Terwilliger, T.C.; Urzhumtsev, A.; Zwart, P.H.; Adams, P.D. Towards automated crystallographic structure refinement with phenix.refine. *Acta Crystallogr. D Biol. Crystallogr.* **2012**, *68*, 352–367. <https://doi.org/10.1107/S0907444912001308>.
25. Mooers, B.H.M. Shortcuts for faster image creation in PyMOL. *Protein Sci.* **2020**, *29*, 268–276. <https://doi.org/10.1002/pro.3781>.
26. Motulsky, H.J. Common misconceptions about data analysis and. *Pharmacol. Res. Perspect.* **2015**, *3*, e00093. <https://doi.org/10.1002/prp2.93>.
27. McGowan, S.; Buckle, A.M.; Mitchell, M.S.; Hoopes, J.T.; Gallagher, D.T.; Heselpoth, R.D.; Shen, Y.; Reboul, C.F.; Law, R.H.P.; Fischetti, V.A.; et al. X-ray crystal structure of the *streptococcal* specific phage lysin PlyC. *Proc. Natl. Acad. Sci. USA* **2012**, *109*, 12752–12757. <https://doi.org/10.1073/pnas.1208424109>.
28. Eijssink, V.G.H.; Matthews, B.W.; Vriend, G. The role of calcium ions in the stability and instability of a thermolysin-like protease. *Protein Sci.* **2011**, *20*, 1346–1355. <https://doi.org/10.1002/pro.670>.
29. Gu, J.; Feng, Y.; Feng, X.; Sun, C.; Lei, L.; Ding, W.; Niu, F.; Jiao, L.; Yang, M.; Li, Y.; et al. Structural and biochemical characterization reveals LysGH15 as an unprecedented "EF-Hand-Like" calcium-binding phage lysin. *PLoS Pathog.* **2014**, *10*, e1004109. <https://doi.org/10.1371/journal.ppat.1004109>.

30. Shin, S.; Yun, Y.S.; Koo, H.M.; Kim, Y.S.; Choi, K.Y.; Oh, B.H. Characterization of a novel ser-cisser-lys catalytic triad in comparison with the classical ser-his-asp triad. *J. Biol. Chem.* **2003**, *278*, 24937. <https://doi.org/10.1074/jbc.M302156200>.
31. Luo, C.H.; Hsu, Y.H.; Wu, W.J.; Chang, K.C.; Yeh, C.S. Phage digestion of a bacterial capsule imparts resistance to two antibiotic agents. *Microorganisms* **2021**, *9*, 794. <https://doi.org/10.3390/microorganisms9040794>.
32. Nelson, D.; Schuch, R.; Chahales, P.; Zhu, S.; Fischetti, V.A. PlyC: A multimeric bacteriophage lysin. *Proc. Natl. Acad. Sci. USA* **2006**, *103*, 10765–10770. <https://doi.org/10.1073/pnas.0604521103>.
33. Shaw, A.; Bott, R.; Vonrhein, C.; Bricogne, G.; Power, S.; Day, A.G. A novel combination of two classic catalytic schemes. *J. Mol. Biol.* **2002**, *320*, 303–309. [https://doi.org/10.1016/S0022-2836\(02\)00387-X](https://doi.org/10.1016/S0022-2836(02)00387-X).
34. Ortega, M.A.; Hao, Y.; Zhang, Q.; Walker, M.C.; Donk, W.; Nair, S.K. Structure and mechanism of the tRNA-dependent lantibiotic dehydratase NisB. *Nature* **2015**, *517*, 509–512. <https://doi.org/10.1038/nature13888>.
35. Wang, I.N.; Smith, D.L.; Young, R. Holins: The protein clocks of bacteriophage infections. *Annu. Rev. Microbiol.* **2000**, *54*, 799–825. <https://doi.org/10.1146/annurev.micro.54.1.799>.
36. Shin, H.; Lee, J.H.; Yoon, H.; Kang, D.H.; Ryu, S. Genomic investigation of lysogen formation and host lysis systems of the *Salmonella* temperate bacteriophage SPN9CC. *Appl. Environ. Microbiol.* **2014**, *80*, 374–384. <https://doi.org/10.1128/AEM.02279-13>.